Optics Letters

Ultrasound-modulated laser feedback tomography in the reflective mode

Kaiyi Zhu,[1] Borui Zhou,[1,2] Yueyue Lu,[1] Puxiang Lai,[3] Shulian Zhang,[1] and Yidong Tan[1,*]

[1]The State Key Laboratory of Precision Measurement Technology and Instruments, Department of Precision Instrument, Tsinghua University, Beijing 100084, China
[2]Department of Electronic and Optical Engineering, Army Engineering University, Shijiazhuang, Hebei 050000, China
[3]Hong Kong Polytechnic University, Department of Biomedical Engineering, Hong Kong SAR, China
*Corresponding author: Tanyd@tsinghua.edu.cn

Received 20 September 2019; accepted 10 October 2019; posted 14 October 2019 (Doc. ID 378351); published 6 November 2019

A novel method of ultrasound-modulated optical tomography (UOT) detection based on the laser feedback technology is proposed in this Letter. The system has advantages such as a simple structure, high sensitivity, and reflective configuration. Effective penetration depths of up to 9 cm and 5 cm in phantom and biological tissues, respectively, have been demonstrated experimentally. The detection capability is comparable with the state of the art in the transmission mode but with a much lower photon consumption. Although a lot remains to be improved, the proposed method is promising for further development toward practical applications.

https://doi.org/10.1364/OL.44.005414

Optical imaging of biological tissues has become increasingly important because of the nonionizing, noninvasive, and excellent functional and morphological contrast it provides [1]. When light travels in the biological tissue, it undergoes strong scattering due to the refractive index mismatch. Hence, photons inside the tissue sample can be classified as ballistic/quasi-ballistic photons and multiply scattered photons. The former can provide a fine resolution but with a limited penetration depth, usually within the optical diffusion limit (~1 mm) [2], which is the case for popular microscopic modalities such as confocal microscopy [3,4], optical coherent tomography [5,6], and two-photon microscopy [7,8]. Multiply scattered photons can also be used for imaging reconstruction, such as in diffuse optical tomography, although the imaging resolution is compromised and highly dependent on the reconstruction model [1,9]. For pure optical imaging techniques, it is inherently a trade-off between the imaging depth and resolution, posing a critical barrier for them to see wider applications.

To improve the image resolution at depths, ultrasound-modulated optical tomography (UOT), also known as the acousto-optic imaging (AOI), has been proposed [10–12]. In this technique, when photons travel through the focal region of the ultrasound transducer within scattering media, the multiply scattered photons are acoustically tagged by the ultrasonically induced particle displacement and refractive index variation [13,14]. As a result, the tagged photons have a frequency shift equal to the ultrasonic driving frequency. By detecting these frequency-shifted photons at each scanning step, an imaging can be reconstructed that reflects the local optical properties. As the tagged photons can be diffusive, UOT can provide an ultrasonically determined resolution at several centimeters deep in the tissue.

Generally, a low signal-to-noise ratio (SNR) is a major challenge in UOT, as the number of photons being tagged and the depth of phase modulation are both weak. A number of techniques, such as the charge coupled device (CCD)-based heterodyne scheme [15,16], Fabry–Perot interferometry [17,18], photorefractive crystal (PRC) interferometry [19,20], and spectral hole burning (SHB) method [21,22], have been developed to enhance the signal detection sensitivity. Note that to enhance the SNR, the tagged photons should be collected as much as possible with a high *etendue*. With this regard, the SHB method has the highest etendue, enabling imaging through a 9-cm-thick phantom by selectively delaying the tagged light to remove the background [22]. However, the apparatus for SHB is bulky and expensive. The PRC-based scheme is relatively compact and cost effective, and it can see through thickness of up to 9.4 cm in tissue-mimicking phantoms with an absorption inclusion embedded at the depth of 4.7 cm [20]. This method, however, is sensitive to the decorrelation of the optical field because of the slow response of the crystal. On the other hand, current UOT systems are mostly in the transmission mode, i.e., the light incidence and collection are at the opposite sites of the studied sample. This is not convenient in practice. The reflection mode detection can solve this problem, but it is more difficult to implement it due to a great number of unmodulated photons. The reported reflection systems are mostly based on CCD cameras [23–26]. For example, with ring-shaped light illumination, methylene-blue-dyed sentinel lymph node embedded at a depth of 13 mm in the chicken breast tissue can be imaged in a coaxial reflection setup [23]. It is also reported in the same work that the performance in the reflection mode is not comparable with the transmission mode.

In recent years, the frequency-shifted laser feedback technology has attracted much attention due to its simple structure, high sensitivity, and capability of auto alignment [27–29].

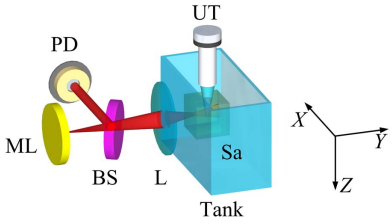

Fig. 1. Schematic diagram of the ultrasound-modulated laser feedback tomography in a reflective configuration. ML, microchip Nd:YVO_4 laser; BS, beam splitter; PD, photodiode; L, lens; UT, ultrasound transducer; Sa, sample.

A great potential has been shown in detecting weak scattered light, and thereby, this technology has seen various applications, such as displacement measurement [30], vibration measurement [31], as well as particle sensing [32] and imaging [33].

In this Letter, this laser feedback technology is proposed as the sensor to probe and demodulate the ultrasound-modulated light in a coaxial reflection configuration. The implementation is rather plain owing to the intrinsic characteristics of the method. In addition, thanks to the ultra-high sensitivity, it is capable of achieving an imaging depth comparable to the state of the art in the transmission method. If further engineered, this method may generate or inspire new advancements in UOT toward practical applications.

The schematic of the experimental system is shown in Fig. 1. The laser-diode-pumped microchip Nd:YVO_4 laser outputs single-longitudinal-mode light at the wavelength of 1064 nm. The output is divided into two beams by the beam splitter. The reflected beam is monitored by a photodiode, while the transmitted part is collimated via a lens and is incident on the front surface of the sample as the probe beam. It has a diameter of 1 mm and an optical intensity of 10 mW. Sinusoidal bursts (central frequency $F_a = 3$ MHz, cycle number = 5000) are produced by a function generator (33250A, Agilent) at a repetition rate of 50 Hz, which are amplified by a power amplifier (LZY-22+, mini circuits) and sent to drive a focused ultrasound transducer (UT; 3-14SF60, EasyNDT). The UT is placed perpendicularly to the propagation of the probe beam, with a focal length of 60 mm and a focal width of 2.16 mm. To maximize the modulation and detection efficiency of light, the UT's focused zone co-aligns with the probing beam, as well as the region of interest in the sample by tuning the mechanical system.

According to the principle of the acousto-optic effect, photons traveling through the ultrasound focal zone are frequency shifted. Part of the backscattered light that contains some tagged photons will return back to the laser cavity, generating a frequency-shifted feedback signal. Sending this signal to a lock-in amplifier (HF2LI, Zurich Instruments) will yield a measurement of the intensity of the ultrasound-modulated photons.

In other words, ultrasonic modulation serves as a frequency-shifted mechanism in a laser feedback system. Since the frequency-shifted photons originate only from the focal zone of the transducer, the amplitude of the obtained signal is thus related to the local optical property [34]. The optical power modulation [30] can be expressed as

Table 1. Key Phantom Parameters for the Monte Carlo Simulation

Simulation	1	2	3	4
Number of photons	1e5	1e5	1e5	1e5
g	0.76	0.76	0.76	0.76
Scattering coefficient (cm^{-1})	10	10	10	10
Absorption coefficient (cm^{-1})	0.1	0.1	0.1	0.1
Target depth (cm)	1	2	3	4
Phantom thickness (cm)	3	4	5	6

$$\frac{\Delta I(F_a)}{I_s} = M_1 \kappa G(F_a) \cos(F_a t - \phi + \phi_s), \tag{1}$$

where ΔI denotes the intensity modulation of the tagged light; I_s is the output power of the solitary laser; M_1 is the ultrasound one-sided modulation depth; κ is the coefficient of the tagged light strength; G is the frequency-dependent amplification factor; F_a is the driving frequency of the UT; ϕ_s is a fixed phase; and ϕ is the phase related to the external cavity length.

Note that due to the low ultrasound modulation efficiency and the strong scattering of light, usually the reflected tagged light is extremely weak and difficult to detect with a desirable SNR. Thanks to the gain factor G, the modulated light can be amplified as high as 10^6 times in our setting, which ensures a high detection sensitivity, even in a coaxial reflection configuration. M_1 is proportional to the quadratic of the acoustic amplitude, which, however, cannot be too high to avoid damage to the transducer and the tissue sample.

The Monte Carlo model [35] is used to simulate the propagation and collection of tagged light in phantoms, with key parameters given in Table 1. In each simulation, two $1 \times 1 \times 1$ cm^3 absorbers are embedded in the phantom with an absorption coefficient of 2 cm^{-1}. The arrangement of the phantom, the absorbers, the light, and the transducer is illustrated in Fig. 2. The sample is scanned at a step of 2 mm along the X-axis. At each step, modulated photons recorded from the reflective and transmissive configurations are compared.

The simulated results are shown in Fig. 3. In the transmission mode, the optical penetration depth is the phantom thickness. In contrast, the penetration depth in the reflection mode is defined as twice the target depth (with respect to the front surface of the sample), considering the round trip for reflected photons. As seen, the two embedded absorbing targets can be clearly resolved, except for the three deepest cases (d, g, and h), where the SNR has approached 1; both the number of "detected" modulated photons and the "imaging" contrast decrease with the penetration depth, regardless of the detection configuration. More importantly, the "imaging" performances, as measured by the number of the modulated photons and the

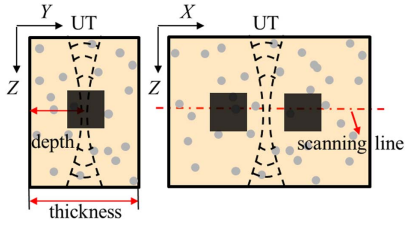

Fig. 2. Illustration of the sample with respect to the light and the ultrasound in simulation.

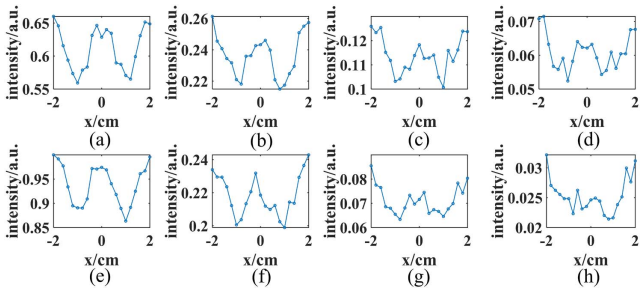

Fig. 3. Simulated intensity profile of modulated photons as a function of the phantom position along the X-axis. (a)–(d) Transmission mode, with penetration depths of 3, 4, 5, and 6 cm, respectively. (e)–(h) Reflection mode, with penetration depths of 2, 4, 6, and 8 cm, respectively.

contrast, are actually comparable across the detection configuration, as long as the penetration depths are close. This suggests that the detection capabilities in the reflection mode and the transmission mode are equivalent to our method, at least in theory. Thus, it is possible to develop a highly sensitive reflection mode UOT by exploiting the laser feedback technology for signal detection.

To confirm the simulated results and the aforementioned hypothesis, experiments with a phantom and a tissue sample were performed. The tissue-mimicking phantom was made by adding 10% (by weight) gelatin (Sigma–Aldrich), and 1% Intralipid (Sigma–Aldrich) into de-ionized water. The mixture was heated, stirred sufficiently, and then solidified, producing a scattering coefficient of 10 cm^{-1} [36,37]. Two $1 \times 1 \times 1$ cm^3 absorbers, with Indian ink added to the phantom matrix material, were embedded in the phantom, as shown in Fig. 4. The absorption coefficient of the absorbers was associated with the ink concentration, which was calibrated in advance. The dimension of the phantom was $7 \times 5 \times 7$ cm^3. The absorbers were positioned in the middle of the X–Z plane with an inter-distance of 1 cm, and the depth of the absorbers was 4.5 cm along the Y-axis. For the tissue experiment, a pork sample was wrapped using thin transparent gelatin gel layers for fixation. Similarly, two $1 \times 1 \times 1$ cm^3 absorbers were embedded in the tissue sample at a depth of 2.5 cm along the Y-axis. In experiment, long bursts of ultrasound (5000 cycles) were applied to generate the ultrasonic modulation. The samples

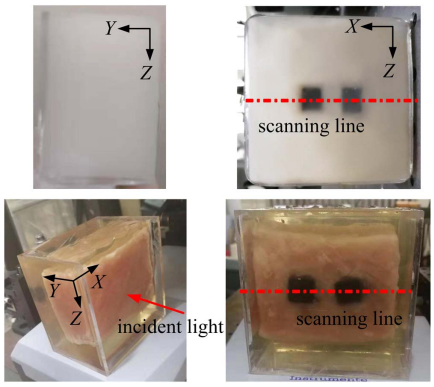

Fig. 4. Arrangement of the phantom and pork tissue samples with respect to the light and the sound. The red dashed lines indicate the scanning direction in the experiment.

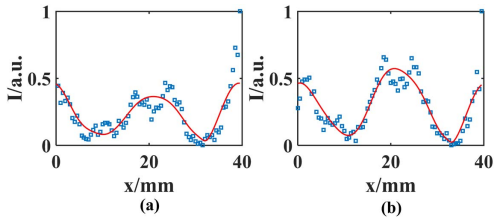

Fig. 5. Experimental results of the one-dimensional scanning. (a) Phantom scanning. (b) Pork tissue scanning; red curve, FFT smoothed result.

were scanned along the dashed lines in Fig. 4 by a precision displacement stage (M511, Physik Instrumente).

The experimental results are shown in Fig. 5. As presented, the detected modulated signals can identify the position and dimension of the two absorbers reliably. The imaged width (along the X-axis) of the two absorbers is ~10 mm, and the gap between them is ~10 mm, which is in agreement with the actual features. The measurement resolution is ~3 mm from the span between the one-fourth and the three-fourths of the contrasts, which is slightly greater than the ultrasound focal width (2.16 mm). Note that these results were obtained in samples with penetration depths of 9 cm (for phantom) and 5 cm (for tissue) in the reflection mode, which is comparable to the maximum penetration depths that have been reported thus far in the transmission mode [20,22], not to mention that the photon budget is much lower in this study.

As long as the ultrasonic bursts were utilized, the resolution along the acoustic propagation direction was compromised in this study. To obtain a two-dimensional (2D) imaging, the transducer was aligned along the light propagation direction, and the scanning stage was set to be perpendicular to the light and ultrasound. A 2D fast Fourier transform (FFT) smoothed map of two $1 \times 1 \times 1$ cm^3 absorbers, embedded at a depth of 1 cm is shown in Fig. 6.

It should be pointed out that the lateral resolution in this study is determined by the ultrasonic focal spot, which can be improved by decreasing the focal length, increasing the element diameter of the transducer, or increasing the ultrasound transducer central frequency. The last parameter, on the other hand, needs to match the selected frequency of the microchip laser. In addition, short ultrasound bursts containing only a few cycles (e.g., <5) of pulses are preferred if imaging resolution along the acoustic resolution is sought for. This, of course, will reduce the ultrasonic modulation efficiency and will demand more

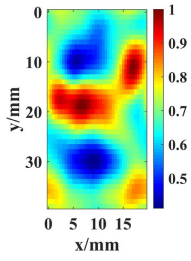

Fig. 6. Two-dimensional imaging of two absorbers embedded at a depth of 1 cm. The blue regions have lower modulated signals due to the increased local absorption coefficient, revealing the position and dimensions of the two targets.

intensive light, which, however, is still way below the laser safety limit (1 W/cm^{-2} @1064 nm) [38].

In conclusion, a reflective configuration with high sensitivity for the UOT signal detection is developed based on a laser feedback technology. Penetration depths of up to 9 cm in a tissue-mimicking phantom and 5 cm in a biological tissue have been demonstrated experimentally. The imaging performance, in terms of the penetration depth, SNR, and contrast, is comparable or even superior to existing UOT implementations, which are mostly in the transmission mode and use a lot more powerful laser source. Therefore, the proposed method, while with a lot to be improved, is promising to advance UOT toward more practical applications.

Funding. National Science Fund for Excellent Young Scholars (51722506); National Natural Science Foundation of China (61775118).

Disclosures. The authors declare no conflicts of interest.

REFERENCES

1. L. V. Wang and H. Wu, *Biomedical Optics: Principles and Imaging* (Wiley, 2007), pp. 1–8.
2. L. V. Wang and S. Hu, Science **335**, 1458 (2012).
3. T. Wilson, *Confocal Microscopy* (Academic, 1990).
4. L. Qiu, D. Liu, W. Zhao, H. Cui, and Z. Sheng, Opt. Express **22**, 21626 (2014).
5. L. Yi, L. Sun, and W. Ding, J. Biomed. Opt. **22**, 106016 (2017).
6. J. F. De Boer, R. Leitgeb, and M. Wojtkowski, Biomed. Opt. Express **8**, 3248 (2017).
7. S. Karpf, M. Eibl, B. Sauer, F. Reinholz, G. Hüttmann, and R. Huber, Opt. Express **7**, 2432 (2016).
8. T. B. Krasieva, J. Ehren, T. O'sullivan, B. J. Tromberg, and P. Maher, Neurochem. Int. **89**, 243 (2015).
9. Y. Hoshi and Y. Yamada, J. Biomed. Opt. **21**, 091312 (2016).
10. D. S. Elson, R. Li, C. Dunsby, R. Eckersley, and M. Tang, Interface Focus **1**, 632 (2011).
11. S. G. Resink, A. C. Boccara, and W. Steenbergen, J. Biomed. Opt. **17**, 040901 (2012).
12. J. Gunther and S. Andersson-Engels, Front. Optoelectron. **10**, 211 (2017).
13. W. Leutz and G. Maret, Phys. B **204**, 14 (1995).
14. M. Kempe, M. Larionov, D. Zaslavsky, and A. Z. Genack, J. Opt. Soc. Am. A **14**, 1151 (1997).
15. M. Gross, "Speckle decorrelation in ultrasound-modulated optical tomography made by heterodyne holography," arXiv: 1606.02902 (2016).
16. M. Gross, P. Goy, and M. Al-Koussa, Opt. Lett. **28**, 2482 (2003).
17. S. Sakadžić and L. V. Wang, Opt. Lett. **29**, 2770 (2004).
18. G. Rousseau, A. Blouin, and J. P. Monchalin, Opt. Lett. **34**, 3445 (2009).
19. G. Rousseau, A. Blouin, and J. P. Monchalin, Opt. Express **16**, 12577 (2008).
20. P. Lai, X. Xu, and L. V. Wang, J. Biomed. Opt. **17**, 066006 (2012).
21. C. Venet, M. Bocoum, J. B. Laudereau, T. Chaneliere, F. Ramaz, and A. Louchet-Chauvet, Opt. Lett. **43**, 3993 (2018).
22. H. Zhang, M. Sabooni, L. Rippe, C. Kim, S. Kröll, L. V. Wang, and P. R. Hemmer, Appl. Phys. Lett. **100**, 131102 (2012).
23. C. Kim, K. H. Song, K. I. Maslov, and L. V. Wang, J. Biomed. Opt. **14**, 024015 (2009).
24. S. Lévêque-Fort, J. Selb, L. Pottier, and A. C. Boccara, Opt. Commun. **196**, 127 (2001).
25. Y. Cheng, S. Li, R. J. Eckersley, D. S. Elson, and M. X. Tang, Biomed. Opt. Express **6**, 63 (2015).
26. M. Hisaka, Appl. Phys. Lett. **88**, 033901 (2006).
27. T. Taimre, M. Nikolić, K. Bertling, Y. L. Lim, T. Bosch, and A. D. Rakić, Adv. Opt. Photon. **7**, 570 (2015).
28. J. Li, H. Niu, and Y. Niu, Opt. Eng. **56**, 050901 (2017).
29. K. Zhu, H. Chen, S. Zhang, Z. Shi, Y. Wang, and Y. Tan, Appl. Sci. **9**, 109 (2019).
30. X. Wan, D. Li, and S. Zhang, Opt. Lett. **32**, 367 (2007).
31. K. Abe, K. Otsuka, and J. Y. Ko, New J. Phys. **5**, 8 (2003).
32. S. Sudo, Y. Miyasaka, K. Nemoto, K. Kamikariya, and K. Otsuka, Opt. Express **15**, 8135 (2007).
33. Y. Tan, W. Wang, C. Xu, and S. Zhang, Sci. Rep. **3**, 2971 (2013).
34. P. Lai, R. A. Roy, and T. W. Murray, Opt. Lett. **34**, 2850 (2009).
35. L. V. Wang, S. L. Jacques, and L. Zheng, Comput. Methods Programs Biomed. **47**, 131 (1995).
36. S. T. Flock, S. L. Jacques, B. C. Wilson, W. M. Star, and M. J. C. Gemert, Lasers Surg. Med. **12**, 510 (1992).
37. P. Lai, X. Xu, and L. V. Wang, J. Biomed. Opt. **19**, 035002 (2014).
38. "Safety of laser products Part 1: Equipment classification and requirements," Standardization Administration of China GB 7247.1-2012.